

Received July 5, 2020, accepted July 20, 2020, date of publication July 27, 2020, date of current version August 13, 2020.

Digital Object Identifier 10.1109/ACCESS.2020.3011970

Ultrasound Image Filtering and Reconstruction Using DCT/IDCT Filter Structure

BARMAK HONARVAR SHAKIBAEI ASLI^{1,3}, (Member, IEEE),
JAN FLUSSER^{2,3}, (Senior Member, IEEE), **YIFAN ZHAO**¹, (Senior Member, IEEE),
JOHN AHMET ERKOYUNCU¹, **KAJOLI BANERJEE KRISHNAN**⁴, **YASIN FARROKHI**⁵,
AND RAJKUMAR ROY⁶, (Member, IEEE)

¹Through-Life Engineering Services Centre, School of Aerospace, Transport and Manufacturing, Cranfield University, Cranfield MK43 0AL, U.K.

²Faculty of Management, University of Economics, 37701 Jindřichuv Hradec, Czech Republic

³Institute of Information Theory and Automation, Czech Academy of Sciences, 18208 Praha 8, Czech Republic

⁴Society for Innovation and Development (SID), Indian Institute of Science, Bengaluru 560012, India

⁵Department of Radiology, School of Medicine, Urmia University of Medical Sciences, Urmia 571478334, Iran

⁶School of Mathematics, Computer Science and Engineering City, University of London, London EC1V 0HB, U.K.

Corresponding author: Barmak Honarvar Shakibaei Asli (barmak@cranfield.ac.uk)

This work was supported in part by the U.K. Engineering and Physical Sciences Research Council (EPSRC) Global Challenges Research Fund (GCRF) Grant: Distributed Intelligent Ultrasound Imaging System for Secure in-community Diagnostics (SecureUltrasound) under Grant EP/R013950/1, which involves Cranfield University, the Indian Institute of Science, the St. John's Research Institute in India, the National Institute of Advanced Studies in India, the City University of London, and Health Education England, and in part by the Praemium Academiae, awarded by the Czech Academy of Sciences, and in part by the Joint Laboratory SALOME 2. The work of Barmak Honarvar Shakibaei Asli was supported by the Czech Science Foundation under Grant 18-26018Y. The work of Jan Flusser was supported by the Czech Science Foundation under Grant GA18-07247S.

ABSTRACT In this paper, a new recursive structure based on the convolution model of discrete cosine transform (DCT) for designing of a finite impulse response (FIR) digital filter is proposed. In our derivation, we start with the convolution model of DCT-II to use its Z-transform for the proposed filter structure perspective. Moreover, using the same algorithm, a filter base implementation of the inverse DCT (IDCT) for image reconstruction is developed. The computational time experiments of the proposed DCT/IDCT filter(s) demonstrate that the proposed filters achieve faster elapsed CPU time compared to the direct recursive structures and recursive algorithms for the DCT/IDCT with Arbitrary Length. Experimental results on clinical ultrasound images and comparisons with classical Wiener filter, non-local mean (NLM) filter and total variation (TV) algorithms are used to validate the improvements of the proposed approaches in both noise reduction and reconstruction performance for ultrasound images.

INDEX TERMS Discrete cosine transform (DCT), inverse discrete cosine transform (IDCT), discrete convolution, finite-impulse filter (FIR), Z-transform, ultrasound images, noise.

I. INTRODUCTION

The DCT has found wide applications in signal and image processing in general, and in data compression, filtering and feature extraction in particular. The DCT has been proved successful at decorrelating and correlating the energy of image data. After decorrelation, each DCT coefficient can be encoded independently without losing compression efficiency since it has a strong 'energy compaction' property in typical applications [1], [2]. In comparison to discrete Fourier transform (DFT), DCT is a transform commonly applied to real valued data (although there are applications and methods where DCT is applied to real and imaginary

components of signals or images separately) and therefore avoids the problem of redundancy. Also, as DCT is derived from DFT, all the desirable properties of DFT (such as the fast algorithm) are preserved. To reduce DCT computational complexities, the development of fast and efficient algorithms for computing 2-D DCT/IDCT becomes increasingly important. Various fast algorithms for computing 2-D DCT were proposed to minimize the computational complexity [3]–[7]. Numerous 1-/2-/3-D DCT architectures have been suggested in the literature [8], [9]. Exploiting the separability principle of the transform, 2-D DCT cores based on the 1-D DCT Row-Column approach are suggested in [10]; yet very few architectures that implement the 3-D DCT can be found. However, there are a variety of DCT of which four are common (DCT-I, DCT-II, DCT-III, and DCT-IV).

The associate editor coordinating the review of this manuscript and approving it for publication was Md. Kamrul Hasan ^{ID}.

Each differs by only a bit, and each has its own usage in particular field. For image reconstruction, DCT II is used to decompose and DCT III is used to reconstruct. Each DCT has its cosine basis kernel which is orthogonal. The most common variant of discrete cosine transform is the type-II DCT, which is often called simply “the DCT”. Its inverse is correspondingly often called simply “the inverse DCT” or “the IDCT”. The N -point DCT-II of a discrete signal, $x(n)$ is given by

$$X_k = c(k) \sum_{n=0}^{N-1} x(n) \cos \left[\frac{\pi}{N} \left(n + \frac{1}{2} \right) k \right], \quad (1)$$

for $k = 0, 1, \dots, N - 1$, where

$$c(k) = \begin{cases} \frac{1}{\sqrt{N}}, & k = 0 \\ \sqrt{\frac{2}{N}}, & \text{otherwise.} \end{cases}$$

The above scale factor can be rewritten in terms of the unit impulse and step functions as $c(k) = \left[\delta(k) + \sqrt{2}u(k-1) \right] / \sqrt{N}$. The inverse 1-D discrete cosine transform (IDCT)-II can be defined as

$$x(n) = \sum_{k=0}^{N-1} c(k) X_k \cos \left[\frac{\pi}{N} \left(n + \frac{1}{2} \right) k \right], \quad (2)$$

for $n = 0, 1, \dots, N - 1$.

Medical ultrasound images are usually corrupted by noise in its acquisition and transmission. Hand-held ultrasound scanners are increasingly being employed at the point of care and used in telemedicine to serve rural population limited access to hospitals [11]. However, image quality of these portable systems are in general poorer than those of standard scanners. They are also often used in scans by physicians rather than by expert sonographers. Thus, the poor image quality is one of the major drawbacks of the ultrasound image due to speckle noise.

There are many despeckling algorithms that consider a log-compression rule and assume the B-mode data which can be modeled by a particular type of double exponential distribution [12]. In general, ultrasound images have two main noise components - electronic noise, modeled as an additive white Gaussian noise, and speckle noise. In raw RF data, speckle noise is multiplicative but in the B-mode image we consider it as an additive noise due to the log transform. Speckle noise is correlated with the signal and is not Gaussian [13]. However, the proposed denoising suppresses up to some extent all additive components regardless of their probability distribution. On the other hand, multiplicative speckle noise is generally more difficult to remove than additive noise, because the intensity of the noise varies with the image intensity [14]. Image noise is usually random, but ultrasound speckle is not random and results from some patterns of constructive and destructive interference shown as bright and dark dots in the image. Sometimes speckle helps to identify the boundaries better in ultrasound images

than without speckle. In addition to speckle, there is thermal noise in ultrasound images arising due to electronics. In this research, the proposed method deals with the additive noise which is pertinent to addressing the image quality of low cost scanners in which noise performance of amplifiers may be low compared to high end scanners. The proposed method also allows for reconstruction after compression which may be necessary in telemedicine (when images will need to be transmitted over limited band widths). Moreover, there is a multiplicative correlated speckle noise in ultrasound images and the main challenge is to reduce it without any loss of finer details of image. The model of the ultrasound images is considered to be the result of the convolution of the point spread function (PSF) of the imaging system with the fetus image function plus additive noise. On the other hand, the fetus image function could be modeled as the multiplication of the original image and speckle noise. Taking this two complex models for PSF and speckle noise into account with the proposed DCT-filter design is a very difficult task and needs more research to be done. However, our proposed DCT filter design is independent as its current form.

As mentioned earlier, the main drawback of ultrasound imaging is related to the low contrast resolution in ultrasound images due to the presence of speckle, which is a form of locally correlated multiplicative noise and generated by the interference of the acoustic energy from randomly distributed structure scatters. Several despeckling methods have been proposed in literature [15], [16]. Different filter families have been defined, each one with peculiar characteristics [17]. One of the most effective methods is commonly referred to as non-local mean (NLM), and has been proposed in [18]. This approach assumes the presence of several similar regions across the image (patches), that can be jointly exploited for regularizing the acquired data [19]. Another successful tool for ultrasound despeckling is the total variation (TV) minimization model [20]. Due to its anisotropy, this technique allows coherent structure enhancement while the dynamic smoothing is controlled by the local behavior of the images. According to this algorithm, reducing the total variation of the image subject to it being a close match to the original image, removes unwanted detail whilst preserving important details such as edges.

The presence of speckle noise affects difficulties on features extraction and quantitative measurement of ultrasound images. Some algorithms would suppress the speckle noise while attempting to preserve the image content using combination of Gaussian filter and DCT approach [21]. Furthermore, the main challenge in image denoising techniques is to remove such noises while preserving the important features and details. Therefore, the reduction of noise is necessary to improve the quality of echographic images and to facilitate its interpretation. A number of methods have been made to reduce noise using various types of filtering. Filtering techniques can be classified as single scale spatial filtering (linear, nonlinear, adaptive methods, etc.) and

multiscale filtering (anisotropic diffusion-based methods, DCT, Wiener, wavelet, curvelet, contourlet, etc.). Mean filtering and Gaussian filtering are the examples of linear methods which blur the sharp edges, destroy lines and suppress the details [22]–[24]. A multiscale approach that aggregates the outputs of DCT filters having different overlapped block sizes is proposed by Pogrebnyak and Lukin [24]. They proposed a two-stage denoising procedure that presumes the use of the multiscale DCT-based filtering with hard thresholding at the first stage and a multiscale Wiener DCT-based filtering at the second stage. They also showed that filtering efficiency depends considerably on DCT coefficient statistics.

In this paper, our approach toward deriving an FIR filter structure is as follows. First, we consider a convolution equation to simplify 1-D DCT based on the flipped input signal as discussed in Theorem 1. Next, we obtain the transfer function of the FIR filter in Z-domain to find a simple filter structure of DCT coefficients generation [25], [26]. This stage of our design paves way for deriving a new and fast algorithm to find a recursive formula to generate the DCT coefficients. Finally, using the orthogonality property of cosine function, we derive the IDCT-II FIR filter structure to recover the original signal based on its limited DCT-II coefficients by applying the same method of transfer function design. Another recursion is proposed for IDCT from transfer function to compute the original signal from its DCT features. Moreover, the proposed FIR filters make an automatic system to accelerate the generated DCT coefficients to apply it for the proposed DCT-based ultrasound image filtering. This paper considers the application in ultrasound images as an example which is motivated by demanding of noise removal from specific fetal images. The developed approach is not applicable only to the context of ultrasound. The context is intentionally selected to serve as an example for a highly complex scenario, where image quality issues are experienced due to speckle noise. This ultimately affects the feature extraction and the quantitative measurement of images. We acknowledge that the developed approach has potential to be applied in a number of other areas including engineering (e.g. nondestructive testing (NDT) inspections for instance, in welded joints) and medical (e.g. abdominal organs, heart, breast, muscles, tendons, arteries and veins and tissue characterization).

The remainder of this paper is organized as follows. In section II, a derivation of a recursive algorithm for 1-D DCT are provided. Section III presents the generalized algorithms for 2-D DCT/IDCT implementation based on FIR filter theory. The experimental results in terms of recent DCT-based algorithms for image filtering and reconstruction are discussed in section IV and conclusions are given in section V.

II. DERIVATION OF A RECURSIVE ALGORITHM FOR 1-D DCT AND IDCT

Before deriving a recursive algorithm for 1-D DCT based on FIR digital filter structure, we show how to get a 1-D

signal transform based on any kernel function using a simple discrete convolution in the following Theorem.

Theorem 1: A discrete transformation of a discrete signal, $f(n)$ of length N , over a kernel function of $g(n, k)$ can be derived by the discrete convolution of the kernel and the flipped signal which is evaluated at $N - 1$.

Proof: The discrete transform for a 1-D signal $f(n)$ of length N with any kernel function of $g(n, k)$, can be written as:

$$F_k = \sum_{n=0}^{N-1} f(n)g(n, k). \tag{3}$$

By changing n to $N - 1 - n$, the above equation can be written as:

$$\begin{aligned} F_k &= \sum_{n=0}^{N-1} f(N - 1 - n)g(N - 1 - n, k) \\ &= \sum_{n=0}^{N-1} f^F(n)g(N - 1 - n, k) \\ &= f^F(n) * g(n, k) \Big|_{n=N-1}, \end{aligned} \tag{4}$$

where $f^F(n)$ is the flipped version of the input signal. Using the definition of 1-D discrete convolution for the above equation, we end up with $\sum_{n=0}^{N-1} f(n)g(n, k) = f^F(n) * g(n, k) \Big|_{n=N-1}$, which completes the proof of Theorem 1. \square

A. FIR FILTER IMPLEMENTATION FOR 1-D DCT-II

By applying Theorem 1 to DCT-II definition in (1) and considering the kernel function as a cosine signal, $g(n, k) = \cos \left[\frac{\pi}{N} \left(n + \frac{1}{2} \right) k \right]$, we get:

$$\begin{aligned} X_k &= c(k) \sum_{n=0}^{N-1} x(n) \cos \left[\frac{\pi}{N} \left(n + \frac{1}{2} \right) k \right] \\ &= c(k) \left\{ x^F(n) * h_k(n) \Big|_{n=N-1} \right\}, \end{aligned} \tag{5}$$

where $h_k(n) = \cos \left[\frac{\pi}{N} \left(n + \frac{1}{2} \right) k \right]$. The function $h_k(n)$ is called the digital filter impulse response [27] which is the same as kernel function $g(n, k)$. Such a system is shown in Fig. 1. The system feeds by a flipped signal and generates the DCT-II coefficients which are sampled at $N - 1$.

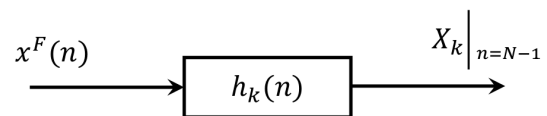


FIGURE 1. A simple FIR filter structure with impulse response $h_k(n)$ for generating DCT-II coefficients from a flipped input signal.

To find the FIR filter structure of the above system, it is easy to obtain the transfer function of the system in

Z-domain ($H_k(z)$). We start to expand the cosine function of $h_k(n)$ as follow:

$$\begin{aligned} h_k(n) &= \cos\left(\frac{\pi nk}{N}\right) \cos\left(\frac{\pi k}{2N}\right) \\ &\quad - \sin\left(\frac{\pi nk}{N}\right) \sin\left(\frac{\pi k}{2N}\right) \\ &= \alpha_k \cos\left(\frac{\pi nk}{N}\right) - \beta_k \sin\left(\frac{\pi nk}{N}\right), \end{aligned} \quad (6)$$

where $\alpha_k = \cos\left(\frac{\pi k}{2N}\right)$ and $\beta_k = \sin\left(\frac{\pi k}{2N}\right)$.

By taking the Z-transform of (6), we can find the transfer function of the FIR filter as:

$$H_k(z) = \frac{z[z - \cos\left(\frac{\pi k}{N}\right)]\alpha_k - z \sin\left(\frac{\pi k}{N}\right)\beta_k}{z^2 - 2z \cos\left(\frac{\pi k}{N}\right) + 1}. \quad (7)$$

Let $\varphi_k = \frac{\pi k}{N}$, then $\alpha_k = \cos\left(\frac{\varphi_k}{2}\right)$ and $\beta_k = \sin\left(\frac{\varphi_k}{2}\right)$. Eq. (7) can be rewritten as:

$$H_k(z) = \frac{\alpha_k - (\alpha_k \cos \varphi_k + \beta_k \sin \varphi_k) z^{-1}}{1 - 2z^{-1} \cos \varphi_k + z^{-2}}. \quad (8)$$

On the other hand, $\alpha_k \cos \varphi_k + \beta_k \sin \varphi_k = \alpha_k$, then Eq. (8) can be simplified as:

$$H_k(z) = \frac{\alpha_k (1 - z^{-1})}{1 - 2z^{-1} \cos \varphi_k + z^{-2}}. \quad (9)$$

The transfer function in Eq. (9) can be implemented as an FIR filter in Fig. 2. This filter contains three delay units and three adders. Moreover, the filter uses three multipliers and two negative feedback. The outputs of filter are sampled at $N - 1$ to generate DCT coefficients for each different values of k . The FIR system is quite simple since we have used the flipped version of the original signal as system input unlike the existing algorithms [3], [28].

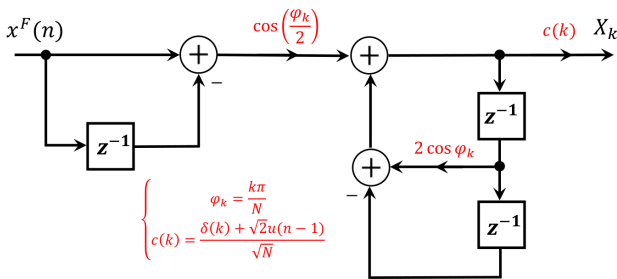


FIGURE 2. DCT network: Recursive FIR filter structure to generate DCT-II coefficients for $k = 0, 1, \dots, N - 1$.

B. FIR FILTER IMPLEMENTATION FOR 1-D IDCT-II

For IDCT-II which is described in (2), it is possible to apply the same theorem and consider the same kernel function with respect to k as the independent variable to get the following convolution:

$$\begin{aligned} x(n) &= \sum_{k=0}^{N-1} c(k)X_k \cos\left[\frac{\pi}{N}\left(n + \frac{1}{2}\right)k\right] \\ &= Y^F(k) * h_n(k) \Big|_{k=N-1}, \end{aligned} \quad (10)$$

where $h_n(k) = \cos\left[\frac{\pi}{N}\left(n + \frac{1}{2}\right)k\right]$ and $Y(k) = c(k)X_k$. Note that here, the impulse response $h_n(k)$ is different with the earlier impulse response $h_k(n)$ because of the concept of the independent variable in signals theory [29]. Taking the Z-transform of $h_k(n)$ with respect to the independent variable k and using the Z-transform of the cosine function [29], the FIR filter transfer function can be written as:

$$H_n(z) = \frac{1 - z^{-1} \cos \omega_n}{1 - 2z^{-1} \cos \omega_n + z^{-2}}, \quad (11)$$

where $\omega_n = \frac{\pi}{N}\left(n + \frac{1}{2}\right)$. The transfer function in (11) can be implemented as an FIR filter which is shown in Fig. 3. This filter also contains three delay units and two adders as well as two multipliers and two negative feedback. The outputs of filter are sampled at $N - 1$ to recover the original signal for each different values of n . The structure also has the flipped version of the DCT coefficients which is multiplied by the scale factor $c(k)$.

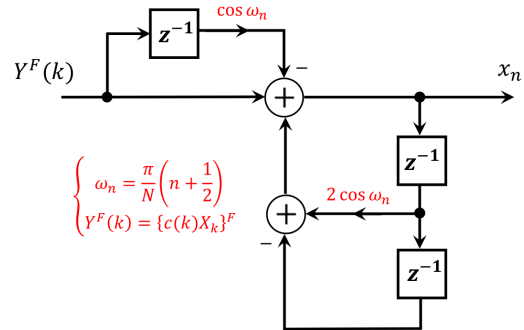


FIGURE 3. IDCT network: Recursive FIR filter structure to reconstruct the original signal from its DCT-II coefficients for $n = 0, 1, \dots, N - 1$.

C. RECURSIVE FORMULAS FOR DCT AND IDCT BASED ON THE PROPOSED ALGORITHMS

The obtained transfer functions in (9) and (11) are in the form of $Y_{out}(z)/X_{in}(z)$. Therefore, by knowing that each delay term in Z-domain such as $z^{-m}Q(z)$, provides a difference form of $q(n - m)$ for all integer m and assumed signal, $q(n)$, we can find a difference relation of the aforementioned equations which are the same as a recurrence formula of the system. For the first transfer function in (9) which is shown as an FIR filter in Fig. 2, we have the following recurrence relation:

$$\begin{aligned} X_k(n) &= c(k) \left\{ \left[x^F(n) - x^F(n - 1) \right] \cos\left(\frac{\varphi_k}{2}\right) \right. \\ &\quad \left. + 2 \cos \varphi_k X_k(n - 1) - X_k(n - 2) \right\}, \end{aligned} \quad (12)$$

where $k = 0, 1, \dots, N - 1$ and $X_k(-1) = X_k(-2) = 0$. The second transfer function in (11) that is shown in Fig. 3, can be converted to a recursive formula for reconstructing the original signal as:

$$\begin{aligned} x_n(k) &= Y^F(k) - (\cos \omega_n) Y^F(k - 1) + 2 \cos \omega_n \\ &\quad \times x_n(k - 1) - x_n(k - 2), \end{aligned} \quad (13)$$

where $n = 0, 1, \dots, N - 1$ and $x_n(-1) = x_n(-2) = 0$. Equation (12) uses n as the independent variable while Eq. (13) presents k as the independent variable for our derived recursive formulas.

III. GENERALIZED ALGORITHMS FOR 2-D DCT/IDCT IMPLEMENTATION

The 2-D DCT-II of an image or a matrix of size $N \times M$ can be defined by

$$X_{k_1, k_2} = c_1(k_1)c_2(k_2) \sum_{n=0}^{N-1} \sum_{m=0}^{M-1} x(n, m) \cos \left[\frac{\pi}{N} \left(n + \frac{1}{2} \right) k_1 \right] \times \cos \left[\frac{\pi}{M} \left(m + \frac{1}{2} \right) k_2 \right], \quad (14)$$

for $k_1 = 0, 1, \dots, N - 1$ and $k_2 = 0, 1, \dots, M - 1$ where $c_1(k_1) = \left[\delta(k_1) + \sqrt{2}u(k_1 - 1) \right] / \sqrt{N}$ and $c_2(k_2) = \left[\delta(k_2) + \sqrt{2}u(k_2 - 1) \right] / \sqrt{M}$.

The 2-D IDCT-II can be formulated as

$$x(n, m) = \sum_{k_1=0}^{N-1} \sum_{k_2=0}^{M-1} c_1(k_1)c_2(k_2)X_{k_1, k_2} \cos \left[\frac{\pi}{N} \left(n + \frac{1}{2} \right) k_1 \right] \times \cos \left[\frac{\pi}{M} \left(m + \frac{1}{2} \right) k_2 \right], \quad (15)$$

where $n = 0, 1, \dots, N - 1$ and $m = 0, 1, \dots, M - 1$. Since the kernels of 2-D DCT/IDCT are separable in (14) and (15), it is easy to design FIR filter for both case based on the 2-D convolution theory and 2-D transfer function $(H_{k_1, k_2}(z_1, z_2))$. z_1 and z_2 are the complex numbers which represent the 2-D Z-transform.

A. 2-D FIR FILTER IMPLEMENTATION FOR 2-D DCT-II

The 2-D DCT-II in (14) can be implemented as a 2-D FIR filter by using the following 2-D convolution:

$$X_{k_1, k_2} = c_1(k_1)c_2(k_2) \left\{ x^F(n, m) * h_{k_1, k_2}(n, m) \right\}_{(n, m)=(N-1, M-1)}, \quad (16)$$

where $h_{k_1, k_2}(n, m) = \cos \left[\frac{\pi}{N} \left(n + \frac{1}{2} \right) k_1 \right] \cos \left[\frac{\pi}{M} \left(m + \frac{1}{2} \right) k_2 \right]$. This 2-D function is the filter impulse response and the system with this impulse response generates the 2-D DCT-II coefficients which are sampled at $(N - 1, M - 1)$.

The same implementation could be applied for (15) to reconstruct the original image from its 2-D DCT-II coefficients. The following convolution is expressed in terms of (k_1, k_2) which are the independent variables here.

$$x(n, m) = Y^F(k_1, k_2) * h_{n, m}(k_1, k_2) \Big|_{(k_1, k_2)=(N-1, M-1)}, \quad (17)$$

where $h_{n, m}(k_1, k_2) = \cos \left[\frac{\pi}{N} \left(n + \frac{1}{2} \right) k_1 \right] \cos \left[\frac{\pi}{M} \left(m + \frac{1}{2} \right) k_2 \right]$ and $Y(k_1, k_2) = c_1(k_1)c_2(k_2)X_{k_1, k_2}$.

B. RECURSIVE FORMULAS FOR THE GENERALIZED 2-D DCT AND IDCT BASED ON THE PROPOSED ALGORITHMS

Based on the kernel separation of 2-D DCT/IDCT, the transfer functions of 2-D FIR filter can be obtained from multiplication of two transfer function described in (9) and (11). Taking the 2-D inverse Z-transform of them, lead us to find the following recurrence relation for computing 2-D DCT:

$$X_{k_1, k_2}(n, m) = c_1(k_1)c_2(k_2) \left\{ \left[x^F(n, m) - x^F(n - 1, m) - x^F(n, m - 1) + x^F(n - 1, m - 1) \right] \times \cos \left(\frac{\varphi_{k_1}}{2} \right) \cos \left(\frac{\varphi_{k_2}}{2} \right) + 2 \cos \varphi_{k_1} \left[X_{k_1, k_2}(n - 1, m) + X_{k_1, k_2}(n - 1, m - 2) \right] + 2 \cos \varphi_{k_2} \left[X_{k_1, k_2}(n, m - 1) + X_{k_1, k_2}(n - 2, m - 1) \right] - 4 \cos \varphi_{k_1} \cos \varphi_{k_2} X_{k_1, k_2}(n - 1, m - 1) - X_{k_1, k_2}(n, m - 2) - X_{k_1, k_2}(n - 2, m) - X_{k_1, k_2}(n - 2, m - 2) \right\}, \quad (18)$$

Fig. 4 shows the implementation of 2D FIR filter to generate 2D DCT coefficients in terms of the original flipped image, $x^F(n, m)$. In this figure, we used z_1^{-1} and z_2^{-1} to show the delay operators for image pixels n and m in time domain, respectively [26]. The circles with a cross symbol inside them (\otimes) represent a multiplier of two signals.

Reconstructing the original image via 2-D IDCT can be found in the following recurrence relation:

$$x_{n, m}(k_1, k_2) = Y^F(k_1, k_2) - 2 \cos \omega_n \left[Y^F(k_1 - 1, k_2) + Y^F(k_1 - 1, k_2 - 2) \right] - 2 \cos \omega_m \times \left[Y^F(k_1, k_2 - 1) + Y^F(k_1 - 1, k_2 - 1) \right] + (4 \cos \omega_n \cos \omega_m) Y^F(k_1 - 1, k_2 - 1) + Y^F(k_1 - 2, k_2) + Y^F(k_1, k_2 - 2) + Y^F(k_1 - 2, k_2 - 2) + (\cos \omega_n) \times x_{n, m}(k_1 - 1, k_2) + (\cos \omega_m) x_{n, m}(k_1, k_2 - 1) - (\cos \omega_n \cos \omega_m) x_{n, m}(k_1 - 1, k_2 - 1), \quad (19)$$

where $\varphi_{k_1} = \pi k_1 / N$, $\varphi_{k_2} = \pi k_2 / M$, $\omega_n = \frac{\pi}{N} \left(n + \frac{1}{2} \right)$, $\omega_m = \frac{\pi}{M} \left(m + \frac{1}{2} \right)$, $X_{k_1, k_2}(i, j) = 0$ and $x_{n, m}(i, j) = 0$ for $i, j = -1, -2$.

IV. EXPERIMENTAL RESULTS

The simulations have been performed using a wide set of captured images based on different fetal scans (normal and anomaly). These scans were performed in a trajectory (axially from head to toe or toe to head followed by sagittally in

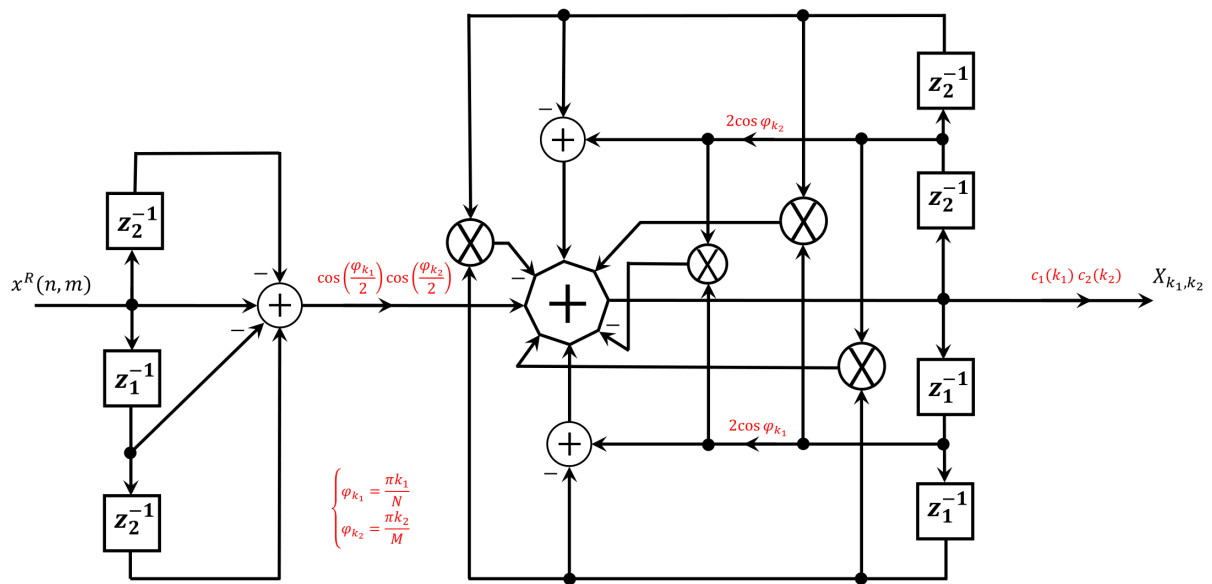


FIGURE 4. Condensed recursive structure for 2-D DCT.

the opposite direction) in a display-less mode. All images were extracted from different sets of videos. Since data are noisy and blurred, we have decided to obtain and present such data for the proposed DCT/IDCT filtering techniques. Fig. 5 shows some of the fetus ultrasound images that we used for our experiments. Note that because of the nature of the ultrasound images according to mean intensity of pixel values, a big part of these data-sets has lower mean intensity. However, the proposed approach can also be applied for any kind of images with different mean intensities.

A. COMPUTATIONAL TIME

In DCT calculation, the time is a critical issue because in general the calculation of DCT coefficients is time expensive and fast algorithms may help a lot. Their importance is even more apparent if we are aware that a typical application of DCT is in image compression where a close-to-real time performance is desirable. There are several properties of DCT have laid the foundation for a faster DCT computation algorithm. We tested the time complexity of the proposed methods (Eqs. (18) and (19)) and compared it to two reference algorithms: the direct recursive structure method [3] and the fast discrete cosine transform (FDCT) algorithm that utilizes the energy compactness and matrix sparseness properties in frequency domain to achieve higher computation performance [30]. The computational complexity of the proposed recursive structures is compared with those of the existing ones [3], [30]. For the fast algorithms of the 2-D DCT, the recursive structures for computing radix-r technique is applied in [3] and the number of additions is reduced to at least 30% of method [31]. The number of multiplications has no reduction and is increased more than 100% which is a drawback of this method. For the second

fast DCT method described in [30], the authors achieved a 40% of reduction in the number of multiplications with no improvement for decreasing of the additions number. To compare those algorithms with the proposed method using digital filter technique, we obtained a 71% and 34% decrement in the number of multiplications comparing to [3] and [30], respectively. In terms of the number of additions, the proposed method has almost a 79% reduction in comparison with [3]. Table 1 shows a comparison of the number of multiplications and additions for computation of DCT coefficients based on three different fast algorithms applied to all test images (size of 400 × 400) which are presented in Fig. 5. Since the proposed algorithm is developed based on the DCT filter structure, there are many reductions in the number of additions and multiplications. The advantage of the proposed technique is in decreasing the number of additions while in [3] by decreasing the number of multiplications, the number of additions starts to increase which is a big drawback of the existing algorithms.

TABLE 1. Number of multiplication and addition operations for computation of DCT coefficients based on three different methods for all fetus ultrasound test images shown in Fig. 5 with size 400 × 400.

Operation	Fast algorithms		Proposed algorithm
	[3]	[30]	
Multiplication	560	245	162
Addition	2450	N/A	520

The experiments were performed on a PC equipped with 3.20 GHz CPU and 64 GB RAM. As can be seen from Fig. 6, the average elapsed time for calculation the full DCT coefficients of ultrasound images shown in Fig. 5 using proposed method is much better than [3] and [30]. One of



FIGURE 5. Some examples of fetus ultrasound data-set images used for experiments. The size of all images is 400×400 .

the most important advantage of the proposed method is eliminating the pre-addition blocks of the existing algorithms. Furthermore, our proposed recursive method gives a direct relationship between the original image as system input and the derived DCT coefficients as the output of the designed FIR filter. We run the same speed test for the average elapsed time of computing original image using its DCT coefficients through IDCT filter structure. Fig. 7 clearly shows that the speed performance of the IDCT recursive method using

Eq. (19) for image reconstruction from a set of finite DCT coefficients is significantly faster than the other mentioned methods.

B. DCT-BASED ULTRASOUND IMAGE FILTERING

The state-of-the-art filters including the DCT-based denoising [22], [24], [32] and the Wiener-based techniques [33] provide filtering performances for complex structure images and large noise variance. Performance characteristics of the

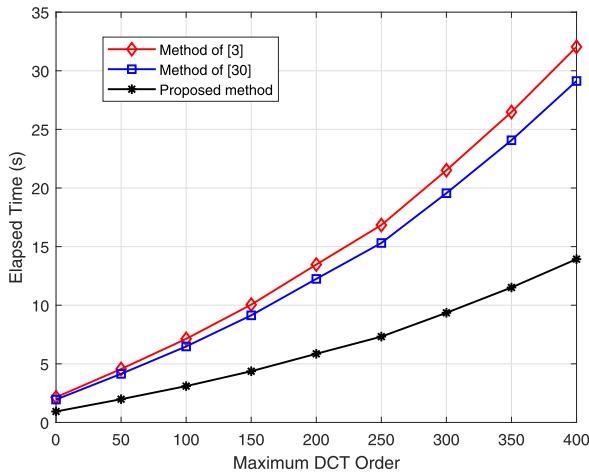


FIGURE 6. Average elapsed CPU times in seconds: full set of DCT coefficients extraction for ultrasound data-sets shown in Fig. 5 using different methods.

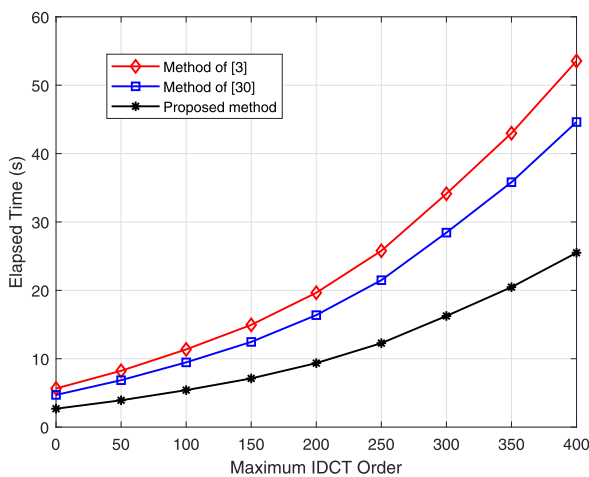


FIGURE 7. Average elapsed CPU times in seconds: full set of IDCT image reconstruction for ultrasound data-sets shown in Fig. 5 using different methods.

state-of-the-art block-matching three-dimensional filter [34] and the Wiener DCT-based filter are very close while the latter filter is simpler and faster.

In this paper, we use the Wiener DCT-based image filtering with hard threshold. As discussed earlier, the speckle noise of medical ultrasound image is modeled as multiplicative noise and non-Gaussian distributed [35] and defined by:

$$g(n, m) = x(n, m)v(n, m) + \eta(n, m), \quad (20)$$

where $g(n, m)$ is an observed noisy image, n and m are the image pixel values, $x(n, m)$ denotes a noise-free image, $v(n, m)$ and $\eta(n, m)$ are multiplicative noise and white Gaussian noise not correlated with $x(n, m)$, respectively. It is suggested that the additive noise has weaker effect than the multiplicative noise of medical ultrasound image. Consequently, (20) can be written as:

$$g(n, m) \approx x(n, m)v(n, m). \quad (21)$$

Laplace and Rayleigh distribution have been used to model the multiplicative noise distribution. For the B-Scan ultrasound images, the logarithmic compression is applied and then (21) is rewritten as:

$$\log g(n, m) \approx \log x(n, m) + \log v(n, m). \quad (22)$$

Then, the multiplicative noise becomes the additive noise and is approximated as an additive zero mean Gaussian noise [35]. It means, we could consider $g(n, m) \approx x(n, m) + v(n, m)$ as the new model of ultrasound images in our coming experiments in logarithmic mode. Similar to Wiener filter, the target is to find an estimate of the noise-free image $\hat{x}(n, m)$ such that it minimizes the mean square error (MSE). Thus, the Wiener DCT-based filter in the DCT domain can be formulated as:

$$\hat{H}_W(k_1, k_2) = \frac{\hat{P}_x(k_1, k_2)}{\hat{P}_x(k_1, k_2) + \lambda(k_1, k_2)\sigma^2}, \quad (23)$$

where $\hat{H}_W(k_1, k_2)$ is an estimate of the frequency response of the Wiener filter and $\hat{P}_x(k_1, k_2)$ is power spectral density estimates of the noise-free image and σ^2 is noise variance since $\lambda(k_1, k_2)$ is proportional to the image size, and $\lambda(0, 0) = 0$ because we assume the Gaussian noise to have zero mean.

We use the DCT instead of the Fourier transform for spectrum calculation in standard Wiener filter, i.e., $\hat{P}_x(k_1, k_2) = X_{k_1, k_2}^2$, where X_{k_1, k_2} is the DCT of a noise-free image. In practice the noise-free image is not accessible to obtain X_{k_1, k_2} . For this reason, the estimate of image power spectral density, $\hat{P}_x(k_1, k_2)$, should be calculated using an observed noisy image. Therefore, the image data has to be pre-filtered to obtain some rough estimate of a noise-free image \hat{X}_{k_1, k_2} and then to calculate $\hat{P}_x(k_1, k_2)$ to implement the Wiener filter in (23).

The last expression for the Wiener DCT-based filter transfer function, Eq. (23), could be simplified assigning the unit gain for all spatial DCT coefficients where $|U(k_1, k_2)| \geq \beta\sigma$ and zero gain otherwise. This results in a hard thresholding technique:

$$H_T(k_1, k_2) = \begin{cases} 1; & |U(k_1, k_2)| \geq \beta\sigma \\ 0; & \text{otherwise,} \end{cases} \quad (24)$$

where β is a control parameter. For our second experiment which is denoising of ultrasound images based on the proposed DCT filter structure, β can be varied from 0 to 1 based on its quasi-optimal value [36]. Fig. 8 illustrates DCT filtering efficiency for three sets of data: first and second rows are the normal fetus, third and fourth rows are the fetal cystic hygroma and the fifth and sixth rows show the fetal hydronephrosis. The sizes of all images are 400×400 pixels. Each image was denoised using a DCT-based Wiener filter led by the proposed FIR filter structure with different level of thresholds ($\beta = 0.1, 0.5, 0.8$). To show the quality of filtered images, we use the statistical-normalization image reconstruction error (SNIRE) in [37] to measure the difference between the original image and the enhanced image by using pixel values. This metric measures the































	Original image	DCT-based denoised image (proposed method)			Wiener filter denoised image
Normal Fetus					
	Threshold level (β)	0.8	0.5	0.1	N/A
	SNIRE	20.6797	17.0367	6.7440	10.1939
	BRISQUE	53.0698	50.2022	45.4849	48.667
					
	Threshold level (β)	0.8	0.5	0.1	N/A
SNIRE	19.8847	16.6770	6.6088	9.4221	
BRISQUE	59.2062	58.5306	44.5435	49.2863	
Fetal Cystic Hygroma					
	Threshold level (β)	0.8	0.5	0.1	N/A
	SNIRE	16.5777	13.5651	4.5613	8.5121
	BRISQUE	59.9236	59.5926	54.4380	55.4829
					
	Threshold level (β)	0.8	0.5	0.1	N/A
SNIRE	15.9925	13.1133	4.3818	7.3997	
BRISQUE	54.5599	53.8146	52.1289	57.1425	
Fetal Hydronephrosis					
	Threshold level (β)	0.8	0.5	0.1	N/A
	SNIRE	19.2214	15.2223	6.3865	8.5244
	BRISQUE	59.6799	53.8941	49.1410	56.6273
					
	Threshold level (β)	0.8	0.5	0.1	N/A
SNIRE	19.5019	15.4862	6.1922	8.4277	
BRISQUE	66.3734	63.0046	45.1998	50.2517	

FIGURE 8. DCT Filtering results for the clinical fetal ultrasound images captured for normal/abnormal fetuses using DCT-based proposed method compared to classical Wiener filter. The last two columns show that the proposed method is performing denoising process better than the Wiener filter.


Image Code	Original image	NLM filter Method	Wiener filter method	TV method	DCT-based method (proposed)
F ₁					
	SNR/CNR (dB)	14.54/1.87	14.58/1.23	14.83/0.86	15.12/0.62
	SNIRE	16.3294	10.4270	8.9243	7.3005
	BRISQUE	41.2454	40.3757	31.3567	26.4126
F ₂					
	SNR/CNR (dB)	16.25/1.52	16.33/1.37	16.52/1.19	16.93/0.84
	SNIRE	14.0771	8.7692	7.9925	6.9443
	BRISQUE	42.9926	38.5410	31.5207	28.7231
F ₃					
	SNR/CNR (dB)	15.75/1.63	15.82/1.42	15.95/1.25	16.28/0.93
	SNIRE	14.6895	9.2463	8.0031	5.7281
	BRISQUE	44.1930	36.0996	32.1947	29.0726
F ₄					
	SNR/CNR (dB)	13.73/2.12	13.95/1.88	14.11/1.53	14.76/1.11
	SNIRE	12.2814	7.9684	7.0111	5.5123
	BRISQUE	50.2615	42.9909	35.0320	30.5061
F ₅					
	SNR/CNR (dB)	15.93/1.95	16.24/1.74	16.85/1.42	17.07/1.20
	SNIRE	15.5811	10.2384	9.2318	7.1829
	BRISQUE	43.3879	39.0791	32.4214	26.7166
F ₆					
	SNR/CNR (dB)	15.71/2.43	15.95/2.19	16.27/1.76	16.58/1.55
	SNIRE	14.1961	8.8572	7.8544	6.7248
	BRISQUE	44.7239	36.7465	33.4985	29.1415

FIGURE 9. Filtering results of the clinical fetus images using four various algorithms: The proposed DCT-based filter is compared with the existing NLM filter, Wiener filter and TV methods. SNR, CNR, SNIRE and BRISQUE as quantitative measurements scores are calculated to show the capability of the proposed method.

average of the squares of the errors which is the average squared difference between the estimated values and the actual value. Moreover, the blind/referenceless image spatial quality evaluator (BRISQUE) is applied to get a score for image measurement from a natural image model [38]–[40]. The score measures the image quality by using the locally normalized luminance coefficients, which were used to calculate the image features. BRISQUE has very low computational complexity, making it well suited for real time applications. BRISQUE features may be used for distortion-identification as well. For this score, a lower value indicates a better subjective quality. These scores show that the quality of enhanced images are improved after DCT filtering processes. Furthermore, we compare the proposed algorithm with classical image denoising method followed by conventional Wiener filter. The last column in Fig. 8 shows the results for the denoised image of the original image illustrated in the first column of the figure by using Wiener filter. The second, third and fourth columns show the proposed DCT-based method to denoise the original images with different level of hard thresholds. It can be seen from the forth and last columns of the figure, when $\beta = 0.1$ the proposed algorithm has better performance and quite good improvements than the classical Wiener filter method. Both SNIRE and BRISQUE criterion confirm the effectiveness of the proposed algorithm.

To show the performance of the proposed filter, we conduct another experiment to compare our method with two well-known denoising algorithms which have been developed for ultrasound despeckling and already mentioned in introduction: NLM filter and the TV method. It should be noted that in the previous experiment, we only compared the proposed method with Wiener filter to obtain an acceptable threshold level for control parameter, β . From the second experiment, it is clear by setting $\beta = 0.1$, we could get a better denoising result for the DCT-based Wiener filter method. However, the third experiment presents a comparison of the proposed method with three different existing algorithms (NLM filter, Wiener filter and TV method) while the threshold level is fixed according to the second experiment ($\beta = 0.1$). Six test images have selected from the fetus ultrasound images shown in Fig. 5 and marked by codes F_1 to F_6 . In addition to the computed SNIRE and BRISQUE values for test images, we use signal-to-noise ratio (SNR) and contrast-to-noise ratio (CNR) in dB to evaluate the capability of the proposed filter against of the existing methods. CNR is a measure used to determine image quality and very similar to SNR. Notice that the image with a high SNR metric might have a low CNR metric. Fig. 9 illustrates the results of the third experiment for ultrasound image denoising based on four various approaches. As can be seen from this figure, the denoising process is improving by SNR increment or reduction of CNR/SNIRE/BRISQUE. The computed image quality metrics in the last column of Fig. 9 confirm that the DCT-based method is performing

significantly better than the existing NLM, Wiener and TV methods.

Another representations of Fig. 9 are shown in Figs. 10, 11, 12 and 13. These four plots show the values of computed SNR, CNR, SNIRE and BRISQUE for the same images as marked by codes F_1 to F_6 . In other words, there are a uniform increment of SNR and a uniform reduction of CNR, SNIRE and BRISQUE for the practical approaches of tested images. The higher SNR values present good quality of the denoised images and the lower CNR, SNIRE and BRISQUE values display a better subjective image quality.

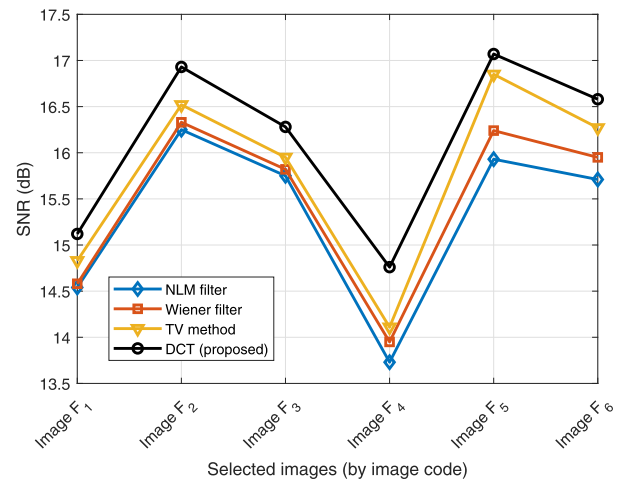


FIGURE 10. Graph of the computed SNR for six images from Fig. 9.

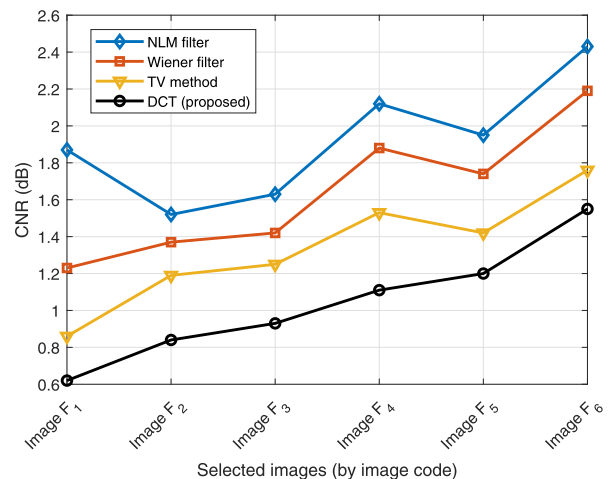


FIGURE 11. Graph of the computed CNR for six images from Fig. 9.

Generally, image quality measures are classified depending on the amount of information available from an original reference image. While full-reference approaches have access to the full-reference image, no information about it is available to no-reference approaches. Besides, there are some standard metrics for measuring image quality as peak signal-to-noise ratio (PSNR) or mean squared error (MSE).

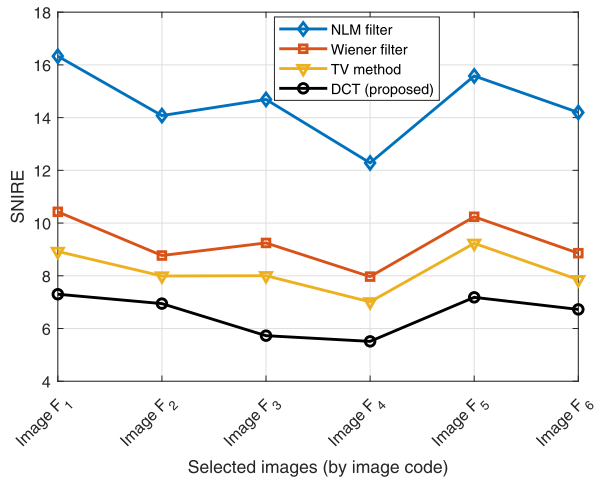


FIGURE 12. Graph of the computed SNIRE for six images from Fig. 9.

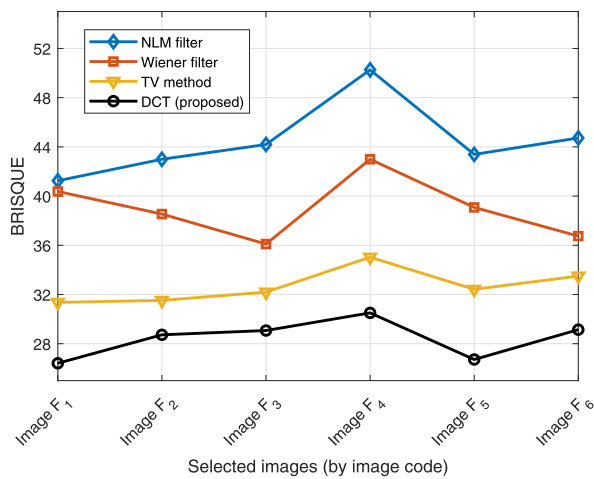


FIGURE 13. Graph of the computed BRISQUE for six images from Fig. 9.

The last experiment of this subsection reports the calculated image quality metrics. We have chosen both PSNR and MSE scores as standard metrics to show image denoising process for NLM, Wiener filter, TV and DCT-based methods. Furthermore, the structural similarity index (SSIM) or the feature similarity index (FSIM) are two perceptual metrics that quantify image quality degradation caused by noise or blur which are taken into account for this experiment [41], [42]. On the other hand, SSIM and FSIM are perception-based models that consider image degradation as perceived change in structural information, while also incorporating important perceptual phenomena, including both luminance masking and contrast masking terms. They are full reference metrics that require two images: a reference image and a processed image. Finally, BRISQUE as the no-reference metric is used to measure the quality of denoised images. Tables 2 and 3 summarize the aforementioned scenario to clarify that the proposed DCT-based filter satisfies the image quality in terms of all three standards, full-reference and no-reference metrics.

TABLE 2. Comparison of the image quality metrics for image F₂ (from Fig. 9) to characterize denoising efficiency using various algorithms.

Image quality scores	NLM filter	Wiener filter	TV method	DCT (proposed)
PSNR	33.4976	35.7800	36.7516	38.1106
MSE	0.000447	0.000264	0.000211	0.000178
FSIM	0.871123	0.883305	0.912467	0.941743
SSIM	0.853645	0.866198	0.889654	0.919882
BRISQUE	42.9926	38.5410	31.5207	28.7231

TABLE 3. Comparison of the image quality metrics for image F₅ (from Fig. 9) to characterize denoising efficiency using various algorithms.

Image quality scores	NLM filter	Wiener filter	TV method	DCT (proposed)
PSNR	32.6476	34.8108	36.1171	39.8124
MSE	0.000544	0.000331	0.000245	0.000109
FSIM	0.854725	0.892770	0.920056	0.960298
SSIM	0.822118	0.851338	0.897116	0.934201
BRISQUE	43.3879	39.0791	32.4214	26.7166

The results in the first and second tables are based on the test images F₂ and F₅, respectively (from Fig. 9). For every one of these criteria, DCT-based filter performs better than all of the other existing approaches being compared.

C. ULTRASOUND IMAGE RECONSTRUCTION USING PROPOSED FILTER STRUCTURE

To show different reconstruction and recognition abilities of the proposed IDCT filter, we carried out the following experiment. Fig.14 shows the same ultrasound images that we used for the second experiment for denoising algorithms. We calculated DCT coefficients using the recursive proposed method by applying Eq. (18) up to order 400 which should theoretically provide a possibility of loss-less reconstruction. We reconstructed the original image by means of Eq. (19) using various DCT coefficients orders (maximum reconstruction orders are 50, 100, 200, 300 and 400 for all images). We used the SNIRE to measure the performance of the proposed IDCT filtering. Lower values of SNIRE means a better reconstruction with less error. As can be seen from Fig.14, by decreasing the DCT reconstruction orders, the SNIRE starts to increase. Besides using SNIRE to measure the error between the original and reconstructed images, the SSIM index is also used to quantify the similarity of images which is a metric to consider image degradation as perceived change in structural information. Higher SSIM matches with a better image reconstruction. The obtained results for SSIM in Fig.14 illustrates that for lower orders the precision quickly decreased.

Fig. 15 shows the image reconstruction error analysis with increasing rate of the DCT orders. This figure also illustrates that an optimal trade-off between the accuracy and complexity is provided by the maximum DCT order between 50 and 100, depending on the data.



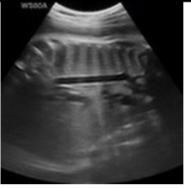
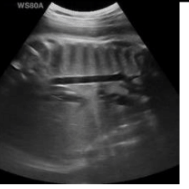
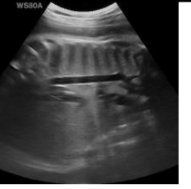
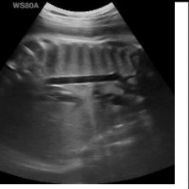




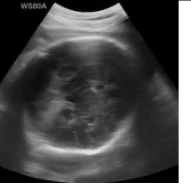
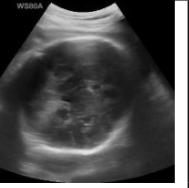
























	Original image	Reconstructed images based on the proposed IDCT filter				
Normal Fetus						
	Max. Order	50	100	200	300	400
	SNIRE	17.2746	11.4128	6.43499	3.97367	0.765523
	SSIM	0.967772	0.986241	0.995663	0.998343	0.999935
						
	Max. Order	50	100	200	300	400
SNIRE	15.5357	11.0797	6.6417	4.16901	1.19042	
SSIM	0.980865	0.990384	0.996564	0.998643	0.999883	
Fetal Cystic Hygroma						
	Max. Order	50	100	200	300	400
	SNIRE	12.2475	5.42537	2.4452	1.43111	0.394929
	SSIM	0.983393	0.996762	0.999324	0.999761	0.999988
						
	Max. Order	50	100	200	300	400
SNIRE	10.6938	5.50489	2.42483	1.29721	0.311768	
SSIM	0.988511	0.996958	0.999395	0.999821	0.999994	
Fetal Hydronephrosis						
	Max. Order	50	100	200	300	400
	SNIRE	16.1456	10.6017	5.34303	3.34015	1.5707
	SSIM	0.949098	0.9787739	0.994671	0.997909	0.999525
						
	Max. Order	50	100	200	300	400
SNIRE	15.7917	10.7213	5.55523	3.33236	0.920456	
SSIM	0.954312	0.979496	0.994569	0.998042	0.999844	

FIGURE 14. Image reconstruction of ultrasound fetus images with different orders with their reconstruction errors using the proposed IDCT filter structure.

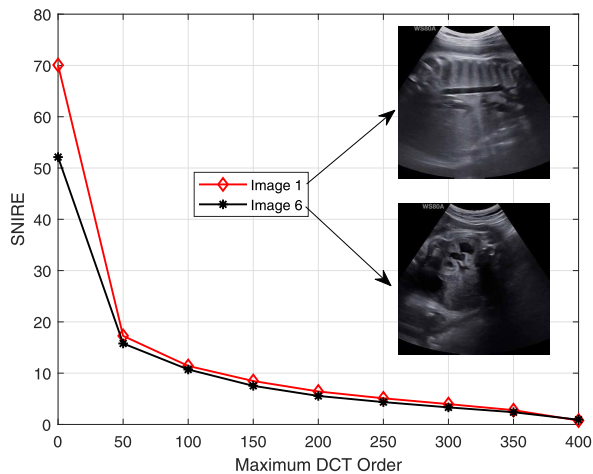


FIGURE 15. Image reconstruction error analysis by increasing DCT orders. In the legend of graph, Images 1 and 6 refer to the original images in the first and last rows of Fig. 14.

V. CONCLUSION

In this paper, a new approach has been proposed for DCT/IDCT calculation based on FIR filter structures and presented its performance on ultrasound image filtering and reconstruction. This approach has been developed using convolution model of DCT to use its Z-transform for designing an FIR digital filter network. The same approach has been used to find a recursive filter to reconstruct ultrasound images using IDCT structure. In order to evaluate the performance of the new filters, a set of normal/abnormal fetus ultrasound images have been applied to test the validity of the proposed algorithms. It has also been shown that filtering efficiency depends considerably on hard thresholding. By choosing a correct threshold level, the denoising results using our method is better than the classical Wiener filter, NLM filter and TV method while the proposed filter is simpler and faster. Additionally, to illustrate the proposed method accuracy, BRISQUE, SNIRE (or MSE/PSNR) and SSIM (or FSIM) indexes showed the image quality scores, the error measurement and the structural similarity in our analysis, respectively. The main advantage of our method is the speed and the ability to perform both lossy and loss-less reconstruction.

REFERENCES

- [1] N. Ahmed, T. Natarajan, and K. R. Rao, "Discrete cosine transform," *IEEE Trans. Comput.*, vol. C-23, no. 1, pp. 90–93, Jan. 1974.
- [2] K. R. Rao and P. Yip, *Discrete Cosine Transform: Algorithms, Advantages, Applications*. San Diego, CA, USA: Academic, 1990.
- [3] C. H. Chen, B. D. Liu, and J. F. Yang, "Direct recursive structures for computing radix-r two-dimensional DCT/IDCT/DST/IDST," *IEEE Trans. Circuits Syst. I, Reg. Papers*, vol. 51, no. 10, pp. 2017–2030, Oct. 2004.
- [4] H. Lee, S. Jin, and J. Jeong, "New fast full search algorithms using DCT coefficients," *IEEE Trans. Consum. Electron.*, vol. 55, no. 2, pp. 845–849, May 2009.
- [5] T. Zong, Y. Xiang, S. Guo, and Y. Rong, "Rank-based image watermarking method with high embedding capacity and robustness," *IEEE Access*, vol. 4, pp. 1689–1699, 2016.
- [6] W. Wan, J. Wu, X. Xie, and G. Shi, "A novel just noticeable difference model via orientation regularity in DCT domain," *IEEE Access*, vol. 5, pp. 22953–22964, 2017.
- [7] R. J. Mstafa, K. M. Elleithy, and E. Abdelfattah, "A robust and secure video steganography method in DWT-DCT domains based on multiple object tracking and ECC," *IEEE Access*, vol. 5, pp. 5354–5365, 2017.
- [8] S. Al-Azawi, O. Nibouche, S. Boussakta, and G. Lightbody, "New fast and area-efficient pipeline 3-D DCT architectures," *Digit. Signal Process.*, vol. 84, pp. 15–25, Jan. 2019.
- [9] I. Jalloh, A. Aggoun, and M. McCormick, "A 3D DCT architecture for compression of integral 3D images," in *Proc. IEEE Workshop SiGNAL Process. Syst. SiPS. Design Implement.*, Oct. 2000, pp. 238–244.
- [10] A. Aggoun and I. Jalloh, "Two-dimensional DCT/IDCT architecture," *IEE Proc.-Comput. Digit. Techn.*, vol. 150, no. 1, pp. 2–10, Jan. 2003.
- [11] O. Noriega, H. Ho, and J. Wright, "The application of hand-held ultrasound scanner in teaching of telemedicine and rural medicine," *Donald School J. Ultrasound Obstetrics Gynecol.*, vol. 8, no. 1, pp. 87–91, 2014.
- [12] J. C. Seabra and J. M. Sanches, "On estimating de-speckled and speckle components from B-mode ultrasound images," in *Proc. IEEE Int. Symp. Biomed. Imag., Nano Macro*, Apr. 2010, pp. 284–287.
- [13] P. Coupe, P. Hellier, C. Kervrann, and C. Barillot, "Nonlocal means-based speckle filtering for ultrasound images," *IEEE Trans. Image Process.*, vol. 18, no. 10, pp. 2221–2229, Oct. 2009.
- [14] P. Hiremath, P. T. Akkasaligar, and S. Badiger, "Speckle noise reduction in medical ultrasound images," in *Advancements and Breakthroughs in Ultrasound Imaging*, G. Gunarathne, Ed. Rijeka, Croatia: IntechOpen, 2013, ch. 8.
- [15] T. Joel and R. Sivakumar, "Despeckling of ultrasound medical images: A survey," *J. Image Graph.*, vol. 1, no. 3, pp. 161–165, 2013.
- [16] F. Baselice, G. Ferraioli, M. Ambrosiano, V. Pascasio, and G. Schirrinzi, "Enhanced Wiener filter for ultrasound image restoration," *Comput. Methods Programs Biomed.*, vol. 153, pp. 71–81, Jan. 2018.
- [17] N. Yahya, N. S. Kamel, and A. S. Malik, "Subspace-based technique for speckle noise reduction in ultrasound images," *Biomed. Eng. OnLine*, vol. 13, no. 1, p. 154, 2014.
- [18] A. Buades, B. Coll, and J. M. Morel, "Image denoising Methods. A new nonlocal principle," *SIAM Rev.*, vol. 52, no. 1, pp. 113–147, Jan. 2010.
- [19] V. Katkovnik, A. Foi, K. Egiazarian, and J. Astola, "From local kernel to nonlocal multiple-model image denoising," *Int. J. Comput. Vis.*, vol. 86, no. 1, pp. 1–32, Jan. 2010.
- [20] L. I. Rudin, S. Osher, and E. Fatemi, "Nonlinear total variation based noise removal algorithms," *Phys. D: Nonlinear Phenomena*, vol. 60, nos. 1–4, pp. 259–268, Nov. 1992.
- [21] S. Riyadi, M. M. Mustafa, A. Hussain, O. Maskon, and I. F. M. Noh, "Quasi-Gaussian DCT filter for speckle reduction of ultrasound images," in *Visual Informatics: Bridging Research and Practice*, H. Badioze Zaman, P. Robinson, M. Petrou, P. Olivier, H. Schröder, and T. K. Shih, Eds. Berlin, Germany: Springer, 2009, pp. 136–147.
- [22] G. Yu and G. Sapiro, "DCT image denoising: A simple and effective image denoising algorithm," *Image Process. Line*, vol. 1, pp. 292–296, Oct. 2011.
- [23] A. Miri, S. Sharifian, S. Rashidi, and M. Ghods, "Medical image denoising based on 2D discrete cosine transform via ant colony optimization," *Optik*, vol. 156, pp. 938–948, Mar. 2018.
- [24] O. B. Pogrebnyak and V. V. Lukin, "Wiener discrete cosine transform-based image filtering," *J. Electron. Imag.*, vol. 21, no. 4, pp. 1–16, 2012.
- [25] K.-H. Chang, R. Paramesran, B. H. S. Asli, and C.-L. Lim, "Efficient hardware accelerators for the computation of tchebichef moments," *IEEE Trans. Circuits Syst. Video Technol.*, vol. 22, no. 3, pp. 414–425, Mar. 2012.
- [26] B. Honarvar Shakibaei Asli, R. Paramesran, and C.-L. Lim, "The fast recursive computation of tchebichef moment and its inverse transform based on Z-transform," *Digit. Signal Process.*, vol. 23, no. 5, pp. 1738–1746, Sep. 2013.
- [27] A. V. Oppenheim and R. W. Schaffer, *Discrete-Time Signal Processing*. Upper Saddle River, NJ, USA: Prentice-Hall, 1989.
- [28] H.-C. Chiang and J.-C. Liu, "A novel DCT-based prefilter structure for efficient digital filter design," *Signal Process.*, vol. 54, no. 3, pp. 249–260, Nov. 1996.
- [29] A. V. Oppenheim, A. S. Willsky, and S. H. Nawab, *Signals & Systems*, 2nd ed. Upper Saddle River, NJ, USA: Prentice-Hall, 1996.
- [30] S. E. Tsai and S. M. Yang, "A fast DCT algorithm for watermarking in digital signal processor," *Math. Problems Eng.*, vol. 2017, pp. 1–7, 2017.
- [31] N. Ik Cho and S. Uk Lee, "Fast algorithm and implementation of 2-D discrete cosine transform," *IEEE Trans. Circuits Syst.*, vol. 38, no. 3, pp. 297–305, Mar. 1991.

- [32] K. Viswanath, J. Mukherjee, and P. K. Biswas, "Image filtering in the block DCT domain using symmetric convolution," *J. Vis. Commun. Image Represent.*, vol. 22, no. 2, pp. 141–152, Feb. 2011.
- [33] S. S. Haykin, *Adaptive Filter Theory*. London, U.K.: Pearson, 2005.
- [34] K. Dabov, A. Foi, V. Katkovnik, and K. Egiazarian, "Image denoising by sparse 3-D transform-domain collaborative filtering," *IEEE Trans. Image Process.*, vol. 16, no. 8, pp. 2080–2095, Aug. 2007.
- [35] S. Gai, B. Zhang, C. Yang, and L. Yu, "Speckle noise reduction in medical ultrasound image using monogenic wavelet and laplace mixture distribution," *Digit. Signal Process.*, vol. 72, pp. 192–207, Jan. 2018.
- [36] R. Öktem, K. Egiazarian, V. V. Lukin, N. N. Ponomarenko, and O. V. Tsymbal, "Locally adaptive DCT filtering for signal-dependent noise removal," *EURASIP J. Adv. Signal Process.*, vol. 2007, no. 1, Dec. 2007, Art. no. 042472.
- [37] Y. Sheng and L. Shen, "Orthogonal Fourier–Mellin moments for invariant pattern recognition," *J. Opt. Soc. Amer. A, Opt. Image Sci.*, vol. 11, no. 6, pp. 1748–1757, Jun. 1994.
- [38] A. Mittal, A. K. Moorthy, and A. C. Bovik, "No-reference image quality assessment in the spatial domain," *IEEE Trans. Image Process.*, vol. 21, no. 12, pp. 4695–4708, Dec. 2012.
- [39] A. Mittal, R. Soundararajan, and A. C. Bovik, "Making a 'completely blind' image quality analyzer," *IEEE Signal Process. Lett.*, vol. 20, no. 3, pp. 209–212, Mar. 2013.
- [40] D. Kundur and D. Hatzinakos, "Blind image deconvolution," *IEEE Signal Process. Mag.*, vol. 13, no. 3, pp. 43–64, May 1996.
- [41] Z. Wang, A. C. Bovik, H. R. Sheikh, and E. P. Simoncelli, "Image quality assessment: From error visibility to structural similarity," *IEEE Trans. Image Process.*, vol. 13, no. 4, pp. 600–612, Apr. 2004.
- [42] L. Zhang, L. Zhang, X. Mou, and D. Zhang, "FSIM: A feature similarity index for image quality assessment," *IEEE Trans. Image Process.*, vol. 20, no. 8, pp. 2378–2386, Aug. 2011.



BARMAK HONARVAR SHAKIBAEI ASLI

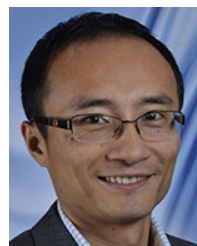
(Member, IEEE) received the Ph.D. degree in electrical engineering from the Department of Electrical Engineering, University of Malaya, Kuala Lumpur, Malaysia, in 2013. He served as a Senior Lecturer with the Azad University of Urmia, Iran, from 1998 to 2009. From 2013 to 2015, he was a Postdoctoral Fellow at the Integrated Light-wave Research Group (ILRG), Faculty of Engineering, University of Malaya,

where he was doing co-supervision for two Ph.D. students in the field of photonics and optics. From 2015 to 2018, he was a Research Fellow at the Department of Image Processing, Institute of Information Theory and Automation, Czech Academy of Sciences, Prague, Czech Republic. He is currently a Senior Research Fellow in intelligent medical imaging and processing and the Project Manager at the School of Aerospace, Transport and Manufacturing, Cranfield University. He has published more than 25 scientific articles in peer-reviewed journals and conference proceedings. His teaching and current research interests include signals and systems, digital filter design, digital image processing, medical image processing, and pattern recognition.



JAN FLUSSER (Senior Member, IEEE) received the M.Sc. degree in mathematical engineering from Czech Technical University, Prague, Czech Republic, in 1985, the Ph.D. degree in computer science from the Czechoslovak Academy of Sciences, in 1990, and the D.Sc. degree in technical cybernetics, in 2001. From 1995 to 2007, he was the Head of the Department of Image Processing. Since 1985, he has been with the Institute of Information Theory and Automation,

Czech Academy of Sciences, where he has been the Director of the Institute of Information Theory and Automation, since 2007. He is currently a Full Professor of computer science with the Faculty of Nuclear Science and Physical Engineering, Czech Technical University, and the Faculty of Mathematics and Physics, Charles University, Prague, where he gives undergraduate and graduate courses on digital image processing, pattern recognition, and moment invariants and wavelets. He has authored or coauthored over 200 research publications in his research areas, including the monographs *Moments and Moment Invariants in Pattern Recognition* (Wiley, 2009) and *2D and 3D Image Analysis by Moments* (Wiley, 2016). His research interests include moments and moment invariants, image registration, image fusion, multichannel blind deconvolution, and superresolution imaging. In 2007, he received the Award of the Chairman of the Czech Science Foundation for the best research project and the Prize of the Academy of Sciences of the Czech Republic for the contribution to image fusion theory. In 2010, he received the SCOPUS 1000 Award. He also received the Felber Medal of the Czech Technical University for excellent contribution to research and education, in 2015.



YIFAN ZHAO

(Senior Member, IEEE) received the B.Eng. and M.Sc. degrees from the Beijing Institute of Technology and the Ph.D. degree in automatic control and system engineering from The University of Sheffield, in 2007. He is currently a Senior Lecturer in data science at the Through-life Engineering Services Institute, Cranfield University, and the Academic Lead of the TES Laboratory. He has over 15 years of experience in signal processing, computer vision,

and artificial intelligence for anomaly detection of complex systems. He has produced more than 100 publications, including 75 peer-reviewed journal articles, more than 25 conference papers, and three book chapters.



JOHN AHMET ERKOYUNCU

is currently the Director of the Through-life Engineering Services Centre, Cranfield University. He is also a Senior Lecturer in digital service engineering. He is the Course Director for the M.Sc. degree in through-life system sustainment. He is currently co-supervising ten Ph.D. projects, eight of which are co-funded by the industry. The projects are focused on enhancing predictability of complex maintenance and improving efficiency of manufacturing and maintenance within the defence, aerospace, pharmaceutical,

health, and automotive sectors. He has published over 70 journal articles and conference papers. His research interests include digital twins, augmented reality, digitalization of degradation assessment, AI, and simulation of complex manufacturing and maintenance procedures. He is a Chartered Engineer, a Fellow of the Higher Education Association, the Chair of the CIRP Research Affiliates, and a member of IET.



KAJOLI BANERJEE KRISHNAN received the bachelor's degree from the St. Stephen's College, Delhi University, and the master's and Ph.D. degrees from IIT Kanpur, all in physics. She is a Physicist by training. She is currently a Senior Research Consultant with the Society for Innovation and Development (SID), Indian Institute of Science, Bengaluru. With 29 years of industrial research experience in imaging system design and applications, she remains deeply committed to the process of ideation, creation, and lab-to-clinical translation of solutions for screening and diagnosis. She has over 50 publications and holds ten filed patents. Her research interests include biomedical ultrasound and optics, robust design, patent evaluation, technology, and IP strategy. She is a Certified Six Sigma Black Belt.



YASIN FARROKHI received the Medical degree and the Master of Public Health degree from the Tehran University of Medical Sciences (TUMS), in 2011. After two years of obligatory period of work as a Family Physician and an Emergency Department Physician, he completed his diagnostic radiology residency at TUMS, from 2013 to 2017. He is currently an Assistant Professor with the Department of Radiology, Urmia University of Medical Sciences, Iran.



RAJKUMAR ROY (Member, IEEE) received the B.Eng. and M.Eng. degrees in production engineering from Jadavpur University, India, and the Ph.D. degree in computing from the University of Plymouth, U.K. He started his career as an Engineer at Tata Motors, pioneered research in through-life engineering services (TES) with Rolls-Royce, BAE Systems, Bombardier Transportation, the Ministry of Defence, and Babcock International, and established an internationally known TES Centre. He joined City, University of London from Cranfield University, where he was the Director of manufacturing. He is currently the Dean of the School of Mathematics, Computer Science and Engineering, City, University of London. His cost engineering and obsolescence research has transformed contemporary understanding of the engineering effort required to design, make, and support high-value products, thus resulting in tools used by BAE Systems, Airbus, the Ministry of Defence, Rolls-Royce, and Ford Motor Company. He is the Founding Editor-in-Chief of the *Applied Soft Computing* journal (Elsevier), from 2000 to 2015, and a Fellow of the CIRP (International Academy for Production Engineers), the Institution of Engineering and Technology (IET), the Institute of Engineering Designers (IED), and the Higher Education Academy (HEA).

...